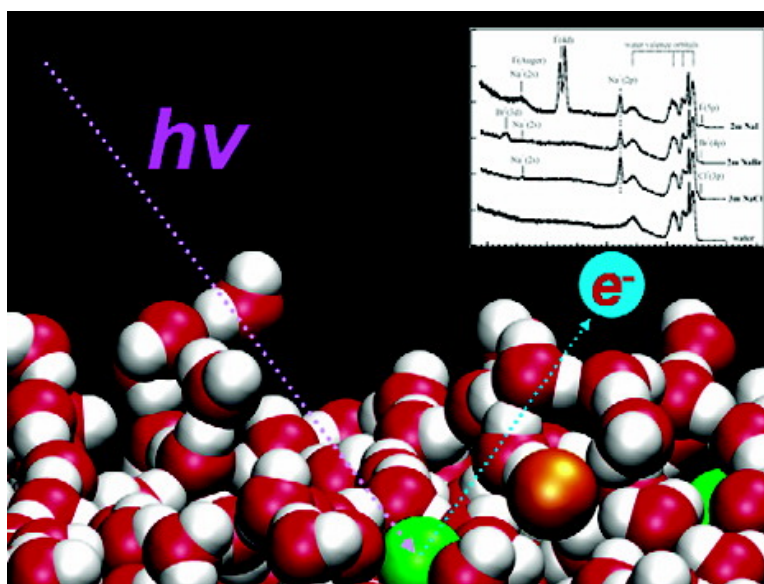


Electron Binding Energies of Aqueous Alkali and Halide Ions: EUV Photoelectron Spectroscopy of Liquid Solutions and Combined Ab Initio and Molecular Dynamics Calculations

Bernd Winter, Ramona Weber, Ingolf V. Hertel, Manfred Faubel,
 Pavel Jungwirth, Eric C. Brown, and Stephen E. Bradforth

J. Am. Chem. Soc., **2005**, 127 (19), 7203-7214 • DOI: 10.1021/ja042908l • Publication Date (Web): 20 April 2005

Downloaded from <http://pubs.acs.org> on March 25, 2009



More About This Article

Additional resources and features associated with this article are available within the HTML version:

- Supporting Information
- Links to the 6 articles that cite this article, as of the time of this article download
- Access to high resolution figures
- Links to articles and content related to this article
- Copyright permission to reproduce figures and/or text from this article

[View the Full Text HTML](#)



ACS Publications
 High quality. High impact.

Electron Binding Energies of Aqueous Alkali and Halide Ions: EUV Photoelectron Spectroscopy of Liquid Solutions and Combined Ab Initio and Molecular Dynamics Calculations

Bernd Winter,^{*,†} Ramona Weber,[†] Ingolf V. Hertel,[†] Manfred Faubel,[‡]
Pavel Jungwirth,^{*,§} Eric C. Brown,[¶] and Stephen E. Bradforth^{*,#}

Contribution from the Max-Born-Institut für Nichtlineare Optik und Kurzzeitspektroskopie, Max-Born-Str. 2A, D-12489 Berlin, Germany, Max-Planck-Institut für Strömungsforschung, Bunsenstr. 10, D-37073 Göttingen, Germany, Institute of Organic Chemistry and Biochemistry, Academy of Sciences of the Czech Republic and Center for Biomolecules and Complex Molecular Systems, Flemingovo nám. 2, 16610 Prague 6, Czech Republic, Department of Chemistry, University of California, Irvine, California 92697-2025, and Department of Chemistry, University of Southern California, Los Angeles, California 90089

Received November 24, 2004; E-mail: bwinter@mbi-berlin.de (B.W.); pavel.jungwirth@uochb.cas.cz (P.J.); bradfort@usc.edu (S.E.B.)

Abstract: Photoelectron spectroscopy combined with the liquid microjet technique enables the direct probing of the electronic structure of aqueous solutions. We report measured and calculated lowest vertical electron binding energies of aqueous alkali cations and halide anions. In some cases, ejection from deeper electronic levels of the solute could be observed. Electron binding energies of a given aqueous ion are found to be independent of the counterion and the salt concentration. The experimental results are complemented by ab initio calculations, at the MP2 and CCSD(T) level, of the ionization energies of these prototype ions in the aqueous phase. The solvent effect was accounted for in the electronic structure calculations in two ways. An explicit inclusion of discrete water molecules using a set of snapshots from an equilibrium classical molecular dynamics simulations and a fractional charge representation of solvent molecules give good results for halide ions. The electron binding energies of alkali cations computed with this approach tend to be overestimated. On the other hand, the polarizable continuum model, which strictly provides adiabatic binding energies, performs well for the alkali cations but fails for the halides. Photon energies in the experiment were in the EUV region (typically 100 eV) for which the technique is probing the top layers of the liquid sample. Hence, the reported energies of aqueous ions are closely connected with both structures and chemical reactivity at the liquid interface, for example, in atmospheric aerosol particles, as well as fundamental bulk solvation properties.

I. Introduction

The interactions between water molecules and dissolved ions are of fundamental interest in understanding aqueous solvation in bulk chemical and biological systems. In addition, aqueous solution interfaces play an important role in atmospheric systems^{1,2} and have been in the focus of research for almost a century.^{3,4} Yet, we are only slowly beginning to understand the structure of aqueous solutions and interfaces on the microscopic level. Experimentally, this is because in situ surface-specific techniques, capable of selectively probing hydrogen bonding and ion adsorption at the aqueous surface, are still relatively

new.^{5,6} Progress toward a molecular picture of the configurations and distributions of inorganic ions near the aqueous solution surface has emerged particularly from nonlinear spectroscopies, such as second harmonic generation (SHG)^{7,8} and sum frequency generation (SFG).^{9–11} Since bulk contributions vanish in these spectroscopies, they are suitable for the study of interfaces. One of the recent results is that there is mounting experimental^{7–10} and theoretical^{12–14} evidence that soft, highly polarizable inorganic anions have a propensity for existing at the top layer of the aqueous solution.

The interest in aqueous salt solutions extends beyond the surface structure. For example, studies of the chemical interactions between dissolved ions and the directly interacting bulk solvent water molecules are required in order to understand ion solvation at the microscopic level. Related is the effect of ions on the long-range bulk hydrogen bond structure, in the textbook

[†] Max-Born-Institut für Nichtlineare Optik und Kurzzeitspektroskopie

[‡] Max-Planck-Institut für Strömungsforschung

[§] Academy of Sciences of the Czech Republic and Center for Biomolecules and Complex Molecular Systems.

[¶] University of California, Irvine.

[#] University of Southern California.

(1) Knipping, E. M.; Lakin, M. J.; Foster, K. L.; Jungwirth, P.; Tobias, D. J.; Gerber, R. B.; Dabdub, D.; Finlayson-Pitts, B. J. *Science* **2000**, *288*, 301.
(2) Finlayson-Pitts, B. J. *Chem. Rev.* **2003**, *103*, 4801.
(3) Onsager, L.; Samaras, N. N. T. *J. Chem. Phys.* **1934**, *2*, 528.
(4) Wagner, C. *Phys. Z.* **1924**, *25*, 474.

(5) Du, Q.; Superfine, R.; Freysz, E.; Shen, Y. R. *Phys. Rev. Lett.* **1993**, *70*, 2313.

(6) Richmond, G. L. *Chem. Rev.* **2002**, *102*, 2693.

(7) Petersen, P. B.; Saykally, R. J. *Chem. Phys. Lett.* **2004**, *397*, 51.

(8) Petersen, P. B.; Johnson, J. C.; Knutsen, K. P.; Saykally, R. J. *Chem. Phys. Lett.* **2004**, *397*, 46.

literature known as structure making and breaking,¹⁵ which refers to the enhancement or weakening of the network structure. Interestingly, using femtosecond mid-infrared nonlinear spectroscopy, such a long-range structural alteration was not confirmed in recent experiments.^{16,17}

Studies of the electronic structure of aqueous solutions are scarce; in fact, the present understanding of solvation is largely based on thermodynamic measurements, for instance, of the solvation free energy or enthalpy associated with the rearrangement of the water molecules around the solute ion (solvation shell). Direct measurements of orbital energies of both solute ions and solvent water molecules, which usually require the determination of the photoelectron kinetic energies, have been hampered experimentally for any high-vapor pressure system. Recently, this situation has changed with the development of the liquid microjet technique, enabling the detection of photoelectrons emerging from the liquid, free from gas-phase collisions, at increased electron-transfer length.^{18,19}

The effect of solvated ions on the electronic structure of water, or vice versa, the effect of solvent water in creating additional electronic states characteristic for the anion-solvate complex (known as charge transfer-to-solvent states, CTTS), is one of the topics that is now being targeted experimentally.^{20–25} Even though the phenomenology of the CTTS process^{26,27} and its relationship to the production of solvated electrons (e_{eq}^-)^{20,28,29} have been known for some time, the general assignment of energies for CTTS transitions over the broad class of aqueous anions is not well established. Further, past workers have speculated that there are Rydberg-like series of such CTTS states;²⁷ however, these higher CTTS bands overlap the liquid conduction band. Consequently, an area of current activity is to map out formation of e_{eq}^- via these direct (conduction band) and indirect (CTTS) pathways.^{23,30,31} To distinguish between the two processes, it would be of great value to accurately determine the energetic position of the conduction band with respect to the ions in aqueous solution.³² This is equivalent to measuring the valence photoemission spectrum, providing the

full distribution of vertical detachment energies resulting from different (anion) solvation configurations. Note that photodetachment *threshold* energies of various aqueous anions, that is, the respective lowest electron detachment energies, have been reported previously;^{33,34} however, derived thresholds are dependent on the experimental sensitivities and extrapolation schemes used.

A related quantity is the ionization potential (IP) of an ion solvated by a well-defined number of water molecules, as measured for gas-phase clusters. Experimental and theoretical studies were focused at elucidating IPs as well as structural features and energetics connected with sequential solvation of ions by a well-defined number of water molecules.^{35–43} Cluster experiments served also as an important tool for calibrating and verifying the applied computational approaches. Whether or not the large cluster size limit and the ionization energy of the bulk solution³² are directly comparable is debatable for the following reasons. First, the convergence to bulk values is relatively slow due to long-range solvent polarization effects; typically, more than 100 water molecules are necessary to reach the onset of bulk behavior.²⁹ Second, the population of solvation sites of the ions (interior vs surface) can change upon moving from clusters to extended systems, although this tends to have only a minor effect on ionization energies.²⁹ Third, the typically considered rigid, low-temperature structure of water clusters differs significantly from that of a solution at ambient conditions.

The present work is a comprehensive treatment of electron binding energies of both alkali cations and halide anions in solution. Vertical ionization energies (VIEs) and vertical detachment energies (VDEs) are measured directly by photoemission from the cations and anions, respectively, in aqueous salt solutions. With a typical 100 eV photon energy, both outer- and inner-shell electron energies can be accessed. In addition, electron binding energies of both anions and cations in water are calculated at three levels of complexity, as far as the inclusion of the solvent is concerned. The first method treats the solvent molecules explicitly within a fractional charge representation, employing sets of geometries from classical molecular dynamics simulations. This allows one to model not only the peaks of the photoelectron spectra but also their width due to solvent fluctuations, which can be compared with experiment. The second method uses the polarizable continuum model. The simplest treatment for the electron binding energies of aqueous ions uses experimental hydration energies in conjunction with the Born equation. Interestingly, a theoretical treatment beyond a thermochemical cycle analysis has not been made before on these prototype ions despite their fundamental interest in the theory of aqueous electrolytes.

II. Experimental and Computational Methods

A. Experimental. A 6 μm diameter liquid microjet is generated in a high-vacuum environment, yielding nearly collisionless evaporation.^{18,19,44} The laminar jet has a temperature of 4 °C and acquires a

- (9) Liu, D. F.; Ma, G.; Levering, L. M.; Allen, H. C. *J. Phys. Chem. B* **2004**, *108*, 2252.
- (10) Shultz, M. J.; Baldelli, S.; Schnitzer, C.; Simonelli, D. *J. Phys. Chem. B* **2002**, *106*, 5313.
- (11) Raymond, E. A.; Richmond, G. L. *J. Phys. Chem. B* **2004**, *108*, 5051.
- (12) Jungwirth, P.; Tobias, D. J. *J. Phys. Chem. B* **2001**, *105*, 10468.
- (13) Jungwirth, P.; Tobias, D. J. *J. Phys. Chem. B* **2002**, *106*, 6361.
- (14) Dang, L. X.; Chang, T. M. *J. Phys. Chem. B* **2002**, *106*, 235.
- (15) Barthel, J. M. G.; Krienke, H.; Kunz, W. *Physical Chemistry of Electrolyte Solutions: Modern Aspects*; Steinkopff, Springer: Darmstadt, New York, 1998; Vol. 5.
- (16) Omta, A. W.; Kropman, M. F.; Woutersen, S.; Bakker, H. J. *Science* **2003**, *301*, 347.
- (17) Kropman, M. F.; Bakker, H. J. *Science* **2001**, *291*, 2118.
- (18) Faubel, M.; Kisters, T. *Nature* **1989**, *339*, 527.
- (19) Winter, B.; Weber, R.; Widdra, W.; Dittmar, M.; Faubel, M.; Hertel, I. V. *J. Phys. Chem. A* **2004**, *108*, 2625.
- (20) Kloepfer, J. A.; Vilchiz, V. H.; Lenchenkov, V. A.; Chen, X. Y.; Bradforth, S. E. *J. Chem. Phys.* **2002**, *117*, 766.
- (21) Vilchiz, V. H.; Kloepfer, J. A.; Germaine, A. C.; Lenchenkov, V. A.; Bradforth, S. E. *J. Phys. Chem. A* **2001**, *105*, 1711.
- (22) Lehr, L.; Zanni, M. T.; Frischkorn, C.; Weinkauff, R.; Neumark, D. M. *Science* **1999**, *284*, 635.
- (23) Barthel, E. R.; Schwartz, B. J. *Chem. Phys. Lett.* **2003**, *375*, 435.
- (24) Crowell, R. A.; Lian, R.; Shkrob, I. A.; Bartels, D. M.; Chen, X.; Bradforth, S. E. *J. Chem. Phys.* **2004**, *120*, 11712.
- (25) Sauer, M. C., Jr.; Shkrob, I. A.; Lian, R.; Crowell, R. A.; Bartels, D. M.; Chen, X.; Suffern, D.; Bradforth, S. E. *J. Phys. Chem. A* **2004**, *108*, 10414.
- (26) Platzmann, R.; Franck, J. Z. *Phys.* **1954**, *138*, 411.
- (27) Blandamer, M. J.; Fox, M. F. *Chem. Rev.* **1970**, *70*, 59.
- (28) Jortner, J.; Ottolenghi, M.; Stein, G. *J. Phys. Chem.* **1964**, *68*, 247.
- (29) Bradforth, S. E.; Jungwirth, P. *J. Phys. Chem. A* **2002**, *106*, 1286.
- (30) Sheu, W.-S.; Rossky, P. J. *J. Phys. Chem.* **1996**, *100*, 1295.
- (31) Chen, X.; Kloepfer, J. A.; Bradforth, S. E.; Lian, R.; Crowell, R. A.; Shkrob, I. A. In preparation.

- (32) Coe, J. V. *Int. Rev. Phys. Chem.* **2001**, *20*, 33.
- (33) Von Burg, K.; Delahay, P. *Chem. Phys. Lett.* **1981**, *78*, 287.
- (34) Delahay, P.; Von Burg, K. *Chem. Phys. Lett.* **1981**, *83*, 250.
- (35) Markovich, G.; Giniger, R.; Levin, M.; Chesnovsky, O. *J. Chem. Phys.* **1991**, *95*, 9416.
- (36) Markovich, G.; Pollack, S.; Giniger, R.; Chesnovsky, O. *J. Chem. Phys.* **1994**, *9344*.
- (37) Choi, J. H.; Kuwata, K. T.; Cao, Y. B.; Okumura, M. *J. Phys. Chem. A* **1998**, *102*, 503.
- (38) Nielsen, S. B.; Masella, M.; Kebarle, P. *J. Phys. Chem. A* **1999**, *103*, 9891.
- (39) Ding, C. F.; Wang, X. B.; Wang, L. S. *J. Phys. Chem. A* **1998**, *102*, 8633.

final velocity of about 125 ms⁻¹. The working pressure is 10⁻⁵ mbar. Photoelectrons pass through a 100 μm orifice, which separates the jet main chamber from the electron detection chamber (10⁻⁹ mbar) housing a hemispherical electron energy analyzer equipped with a single electron multiplier detector. Highly demineralized water was used, and salts were of highest purity commercially available (Aldrich).

The photoemission measurements were performed at the MBI undulator beamline (U125) at the synchrotron radiation facility, BESSY, Berlin. This beamline delivered up to 180 eV photon energies at an energy resolution better than 6000. For the present experiments, the resolution was reduced in favor of the photoemission signal to about 100 meV, which is sufficient since the intrinsic width of the liquid features is typically >0.5 eV. At a photon flux of about 4 × 10¹²/s per 0.1 Å ring current, count rates on the order of 10–100 counts/s at peak maximum were obtained. Under these conditions, the acquisition time of a typical photoemission spectrum (at the signal-to-noise level as presented here) is about 60 min. The synchrotron light intersects the laminar liquid jet at normal incidence, and electron detection is normal to both the jet direction and the light polarization vector.¹⁹

B.1. Computational Methods. The gas-phase ionization energies of all the ions under study were evaluated at the MP2 and CCSD(T) levels. Favorable comparison to experimental gas-phase values for ionization and detachment energies at CCSD(T) shows that virtually all electron correlation is recovered and the residual error is small. In fact, the MP2 approach already provides satisfactory results. To estimate deeper level electron binding energy features in the photoelectron spectra, the gas-phase s → p excitation energies of the ns²np⁵ alkali dications and neutral halogen atoms were computed by means of the time-dependent density functional (TD-DFT) approach employing the hybrid B3LYP functional.

For the study of ionization of alkali cations and detachment of halide anions in bulk liquid water, two different basic strategies were adopted. The first treats the structured electrostatic potential due to the water molecules around the ion explicitly, while the second employs a polarizable continuum model.

For the explicit treatment of the solvent, we employ an approach elaborated in an earlier publication by two of us.²⁹ We start with a classical molecular dynamics (MD) simulation. A single cation or anion is surrounded by 864 water molecules in a box of roughly 30 × 30 × 30 Å, and periodic boundary conditions are applied. Simulations are performed at 300 K at a constant pressure of 1 atm. The polarizable POL3 model of water and a polarizable model for all ions have been employed.^{45–49} The ion polarizabilities used are: 0.24 for Na⁺, 0.98 for F⁻, 3.25 for Cl⁻, 4.53 for Br⁻, and 6.9 Å³ for I⁻.^{48,49} An interaction cutoff of 12 Å has been used, and long-range Coulomb interactions have been summed up via the particle mesh Ewald algorithm.⁵⁰ Simulations have been run for 500 ps after 250 ps of equilibration; 500 geometries, corresponding to snapshots along the MD trajectory separated by 1 ps, have been saved for further calculations. In the second step, ab initio MP2 calculations, with basis sets described in detail below, for the ground state anion and neutral states of the embedded solute are performed for each of the 500 geometries saved along the

Table 1a. Measured Electron Binding Energies ($E_{\text{aq}}^{\text{PES}}$) and Peak Widths (fwhm) of Aqueous Cations (for comparison, the ionization and detachment energies (E_{g}) of the corresponding gas-phase ions are also shown)

cation		$E_{\text{g}}(\text{M}^+)$ (eV)	$E_{\text{aq}}^{\text{PES}}(\text{M}^+)$ (eV)	fwhm _{aq} (eV)
Li	1s	75.64 ^a	60.4 ± 0.07	1.4 ± 0.20
Na	2p	47.28 ^a	35.4 ± 0.04	1.1 ± 0.03
		47.45 ^a		
	2s	80.07 ^a	68.0 ± 0.15	3.1 ± 0.50
K	3p	31.62 ^a	22.2 ± 0.06	1.4 ± 0.20
		31.89 ^a		
	3s	47.81 ^a	~38	
Rb	4p	27.29 ^a	<i>d</i>	
Cs	5p	23.14 ^b	<i>d</i>	<i>d</i>
	5s	38.98 ^c	<i>d</i>	<i>d</i>
	4d _{5/2}	88.55 ^b	80.6 ± 0.03	1.1 ± 0.05
	4d _{3/2}		82.9 ± 0.04	1.3 ± 0.06

^a From ref 77. ^b From ref 78. ^c From sum of atomic transition line⁷² and gas-phase electron affinity.⁷⁸ ^d Not observed.

classical MD trajectory. This ensures fair statistics for the vertical binding energy. All 864 water molecules in the unit cell were represented by fractional point charges of -0.82 for oxygen and 0.41 for hydrogen.⁵¹

The photoelectron (PE) spectrum, subject to the energy of the ionizing radiation, includes electron ejection from all orbitals of the atomic system. In general, in a solution environment, the formal degeneracy of the p orbitals is removed even in the absence of the spin-orbit operator. For alkali cations, except lithium, and all halide anions, ejection takes place from the highest occupied orbital of p symmetry. Thus, the energy corresponding to ejection from each of the broken-degeneracy orbitals must be computed. For each of the MD snapshots, we have actually evaluated the energies of all the three subcomponents, corresponding to electron removal from one of the three valence p orbitals of the ion. In previous work on iodide, vertical detachment energies for different solvent configurations were displayed in a histogram, but these included only ejections from the highest lying p orbital.²⁹ To simulate the liquid PE spectra here, we have included all possible promotions. For iodide, this shifts the median vertical detachment energy from 7.05 to 7.20 eV (Table 2). We note that although an unrestricted wave function is being used for the neutral, which artificially lifts the degeneracy of the p orbitals in the gas phase, the presence of the solvent is a stronger perturbation, as evidenced by the observation of equivalent splittings in a CIS calculation on the anion.

A continuum treatment of the solvent was also evaluated. We have employed the polarizable dielectric continuum model (PCM) by Tomasi et al. as implemented in Gaussian 98.⁵² Energies for both ground state cation and dication, or both anion and neutral, are calculated in independently self-consistently determined spherical cavities with a dielectric constant for the continuum appropriate for water. Therefore, all states are fully relaxed within the continuum model.

For gas phase and both solution approaches, the electronic structure computations are performed as follows. For the cations, a cc-pV5Z basis set is used for Li⁺ and Na⁺.⁵³ For K⁺, we use a 6-311g(2d,f)⁵³ and for Rb⁺ a Sadlej pVTZ basis.⁵³ For Cs⁺, the well-tempered basis set of Huzinaga et al. was employed.⁵⁴ For the anions, as in our previous study, we have employed augmented triple-ζ plus double polarization correlation-consistent quality basis sets. For fluoride, chloride, and

- (40) Steel, E. A.; Merz, K. M.; Selinger, A.; Castleman, A. W. *J. Phys. Chem.* **1995**, *99*, 7829.
 (41) Combariza, J. E.; Kestner, N. R.; Jortner, J. *Chem. Phys. Lett.* **1993**, *203*, 423.
 (42) Perera, L.; Berkowitz, M. L. *J. Chem. Phys.* **1993**, *99*, 4222.
 (43) Dang, L. X.; Garret, B. C. *J. Chem. Phys.* **1993**, *99*, 2972.
 (44) Faubel, M.; Steiner, B.; Toennies, J. P. *J. Chem. Phys.* **1997**, *106*, 9013.
 (45) Caldwell, J.; Kollman, P. A. *J. Phys. Chem.* **1995**, *99*, 6208.
 (46) Caldwell, J.; Dang, L. X.; Kollman, P. A. *J. Am. Chem. Soc.* **1990**, *112*, 9144.
 (47) Pearlman, D. A.; Case, D. A.; Caldwell, J. W.; Ross, W. S.; Cheatham, T. E.; Debolt, S.; Ferguson, D.; Seibel, G.; Kollman, P. *Comp. Phys. Commun.* **1995**, *91*, 1.
 (48) Dang, L. X. *J. Chem. Phys.* **1999**, *110*, 1526.
 (49) Markovich, G.; Perera, L.; Berkowitz, M. L.; Cheshnovsky, O. *J. Chem. Phys.* **1996**, *105*, 2675.
 (50) Essmann, U.; Perera, L.; Berkowitz, M. L.; Darden, T.; Lee, H.; Pedersen, L. G. *J. Chem. Phys.* **1995**, *103*, 8577.

- (51) Berendsen, H. J. C.; Grigera, J. R.; Straatsma, T. P. *J. Phys. Chem.* **1987**, *91*, 6269.
 (52) Cossi, M.; Barone, V.; Cammi, R.; Tomasi, J. *Chem. Phys. Lett.* **1996**, *255*, 327.
 (53) EMSL. Basis sets were obtained from the Extensible Computational Chemistry Environment Basis Set Database, Version 02/25/04, as developed and distributed by the Molecular Science Computing Facility, Environmental and Molecular Sciences Laboratory, which is part of the Pacific Northwest Laboratory, P.O. Box 999, Richland, WA 99352, USA.
 (54) Huzinaga, S.; Klobukowski, M. *Chem. Phys. Lett.* **1993**, *212*, 260.

Table 1b. Measured Electron Binding Energies ($E_{\text{aq}}^{\text{PES}}$) and Peak Widths (fwhm) of Aqueous Anions (for comparison, the ionization and detachment energies (E_{g}) of the corresponding gas-phase ions are also shown)

anion		$E_{\text{g}}(\text{A}^-)$ (eV)	$E_{\text{aq}}^{\text{PES}}(\text{A}^-)$ (eV)	fwhm _{aq} (eV)
F	2p	3.40, ^a 3.45 ^b	8.7 ^e , 9.8 ^f	
	2s	24.3 ^b		
Cl	3p	3.61, ^a 3.72 ^b	9.6 ± 0.07 8.7 ± 0.1	0.6 ± 0.20
	3s	no atomic line	g	
Br	4p	3.36, ^a 3.82 ^b	8.8 ± 0.06 8.1 ± 0.1	0.9 ± 0.20
	4s	13.87 ^c	g	
I	3d _{5/2}	no atomic lines	73.2 ± 0.07	1.2 ± 0.10
	3d _{3/2}		74.3 ± 0.09	1.1 ± 0.10
	5p	3.06, ^a 4.00 ^b	7.7 ± 0.20 8.8 ± 0.20 7.3 ± 0.1	0.8 ± 0.30 1.1 ± 0.30
	5s	13.23 ^b (15.10 ^d) (57.41 ^d)	g	
	4d _{5/2}		53.8 ± 0.03	1.0 ± 0.02
	4d _{3/2}		55.5 ± 0.03	1.0 ± 0.02

^a From ref 79. ^b From sum of atomic transition line⁷² and gas-phase EA.⁷⁹
^c From sum of atomic transition line⁷⁷ and gas-phase electron affinity.⁷⁹
^d From LDA calculations in ref 64. ^e From ref 66. ^f Estimated from ref 65.
^g Not observed.

bromide, we use the standard aug-cc-pVTZ basis set.⁵³ For iodide, we employ a similar quality basis and a “small core” pseudopotential⁵⁵ as defined by Combariza.⁵⁶ For chloride and iodide, these bases are further augmented to enable simultaneous calculation of the CTTS levels for these aqueous anions.²⁹ For chloride, a very diffuse sp even-tempered set⁵⁷ is added, and an identical d set is added beyond that for iodide, each with six exponents forming a geometric series with a factor of 5 and lowest exponent of $2.35 \times 10^{-6} \text{ au}^{-2}$. These extremely diffuse functions have little effect ($\sim 7 \text{ meV}$ for chloride) in the computed electron binding energies, thus, they have not been included for fluoride or bromide. For the alkali dication and halogen neutral gas-phase excitations computed with the TD-DFT approach, we simply remove all diffuse functions from the basis. The diffuse functions are not required for the description of the neutrals, moreover, this way the desired $s \rightarrow p$ excitation, which lies close to the neutral ionization continuum, shows up as a low-lying excited state. Finally, note that the calculations do not explicitly include the spin-orbit interactions. All ab initio calculations were performed using Gaussian 98.⁵⁸ The MD simulations have been carried out using the Amber7 program package.⁵⁹

B.2. Binding Energies Estimated from Experimental Solvation Free Energy. Photoionization probes vertical ionization energies as opposed to adiabatic energies, accessed in the thermodynamic treatment

(55) LaJohn, L. A.; Christiansen, P. A.; Ross, R. B.; Atashroo, T.; Ermler, W. C. *J. Chem. Phys.* **1987**, *87*, 2812.

(56) Combariza, J. E.; Kestner, N. R.; Jortner, J. *J. Chem. Phys.* **1994**, *100*, 2851.

(57) Chen, H. Y.; Sheu, W. S. *J. Am. Chem. Soc.* **2000**, *122*, 7534.

(58) Frisch, M. J.; Trucks, G. W.; Schlegel, H. B.; Scuseria, G. E.; Robb, M. A.; Cheeseman, J. R.; Zakrzewski, V. G.; Montgomery, J. A.; Stratmann, R. E.; Burant, J. C.; Dapprich, S.; Millam, J. M.; Daniels, A. D.; Kudin, K. N.; Strain, M. C.; Farkas, O.; Tomasi, J.; Barone, V.; Cossi, M.; Cammi, R.; Mennucci, B.; Pomelli, C.; Adamo, C.; Clifford, S.; Ochterski, J.; Petersson, G. A.; Ayala, P. Y.; Cui, Q.; Morokuma, K.; Malick, D. K.; Rabuck, A. D.; Raghavachari, K.; Foresman, J. B.; Cioslowski, J.; Ortiz, J. V.; Stefanov, B. B.; Liu, G.; Liashenko, A.; Piskorz, P.; Komaromi, I.; Gomperts, R.; Martin, R. L.; Fox, D. J.; Keith, T.; Al-Laham, M. A.; Peng, C. Y.; Nanayakkara, A.; Gonzalez, C.; Challacombe, M.; Gill, P. M. W.; Johnson, B. G.; Chen, W.; Wong, M. W.; Andres, J. L.; Head-Gordon, M.; Replogle, E. S.; Pople, J. A. *Gaussian 98*; Gaussian Inc.: Pittsburgh, PA, 1998.

(59) Case, D. A.; Pearlman, D. A.; Caldwell, J. W.; Cheatham, T. E., III; Simmerling, C. L.; Darden, T. A.; Merz, K. M.; Stanton, R. V.; Cheng, A. L.; Vincent, J. J.; Crowley, M.; Tsui, V.; Gohlke, H.; Radmer, R. J.; Duan, Y.; Pitera, J.; Massova, I.; Seibel, G. L.; Singh, U. C.; Weiner, P. K.; Kollman, P. A. *AMBER 7*; University of California, San Francisco, 2002.

of fully relaxed states. To connect these quantities, we consider the two processes: (i) $M_{\text{aq}}^+ + h\nu \rightarrow M_{\text{aq}}^{2+} + e_{\text{vac}}$ and (ii) $A_{\text{aq}}^- + h\nu \rightarrow A_{\text{aq}}^{\circ} + e_{\text{vac}}$ of cationic and anionic photoionization. The difference in energy between the left (initial state i) and right side (final state f), which corresponds to adiabatic ionization energy, is given by the difference of the respective solvation free energies, $E_{\text{g}} + (\Delta G_i^{\text{cav}} - \Delta G_f^{\text{cav}})$.⁶⁰ Here, E_{g} is the gas-phase ionization energy, and typically ΔG_i is known experimentally and ΔG_f has not been accurately determined. An estimate for the magnitude of ΔG_f compared to that of ΔG_i may be established from a dielectric continuum cavity model, through the Born equation:^{61–63}

$$\Delta G^{\text{cav}} = -(z^2 e^2 / 8\pi\epsilon_0 R)(1 - 1/\epsilon_{\text{st}})$$

where ΔG^{cav} is the electrostatic free energy, assuming electronic polarization of a continuum solvent about a charge ze in a spherical cavity of radius R , with ϵ_0 and ϵ_{st} being the static permittivity of vacuum and of the dielectric medium, respectively. For anions, the final state is neutral, so ΔG_f^{cav} is expected to be negligible, so $(\Delta G_f^{\text{cav}} - \Delta G_i^{\text{cav}}) \approx -\Delta G_i^{\text{cav}}$; for cations $(\Delta G_f^{\text{cav}} - \Delta G_i^{\text{cav}}) \approx +3\Delta G_i^{\text{cav}}$.⁶⁰ We call this adiabatic ionization estimate $E_{\text{aq}}^{\text{thermo}}$, and it is computed as $E_{\text{g}} - \Delta G^{\circ}$ for anions and $E_{\text{g}} + 3\Delta G^{\circ}$, respectively, using experimental solvation free energies (rather than values from the Born equation itself) for the monovalent cations and anions, respectively.⁵⁶ Comparison of $E_{\text{aq}}^{\text{thermo}}$, which corresponds to fully relaxed final states, to the experimental $E_{\text{aq}}^{\text{PES}}$ is probably not realistic as the time scale of the (vertical) photoionization process is faster than the relaxation of the solvent dipoles (nuclear polarization), which is included in the Born formula as well as the relaxation of the electronic polarization. For cations, it turns out that this discrepancy is relatively small, which may be attributed to the fact that water molecules are already suitably arranged around a positive charge on vertical transformation to the final states, and the nuclear part of the polarization response is proportionately smaller. This is not true for anionic ionization, however, where the final state is neutral and considerable nuclear relaxation will take place, and thus this simple picture is more likely false.

III. Results

A. Photoemission Measurements. Figure 1 contrasts photoemission spectra of aqueous sodium halide solutions for different anions (2 m NaI, 2 m NaBr, and 3 m NaCl) and of pure liquid water for comparison. Higher NaCl concentration is used to enhance the Cl^- signal, which strongly overlaps with the water leading edge. Each spectrum was obtained for 100 eV photon energy; the intensities were normalized to the liquid H_2O $1b_1$ emission signal (see label), and traces are vertically displaced for clarity. Electron binding energies are presented relative to vacuum (11.16 eV for the $1b_1$ orbital of liquid water).¹⁹ Water gas-phase contributions in the spectra result from the continuous H_2O evaporation of the liquid surface, and the broad signal background arises from secondary electrons (inelastic scattering in the bulk liquid) while specific, discrete electron energy losses lead to additional spectral structures.¹⁹ The characteristic emissions from the liquid water valence orbitals, $2a_1$, $1b_2$, $3a_1$, and $1b_1$, as marked in the top panel, are continued to be seen at the identical energies in the solution spectra. Emission from aqueous sodium is observed at 68.0 and

(60) Weber, R.; Winter, B.; Schmidt, P. M.; Widdra, W.; Hertel, I. V.; Dittmar, M.; Faubel, M. *J. Phys. Chem. B* **2004**, *108*, 4729.

(61) Born, M. *Z. Phys.* **1920**, *1*, 45.

(62) Marcus, Y. *Chem. Rev.* **1988**, *88*, 1475.

(63) Lundholm, M.; Siegbahn, H.; Holmberg, S.; Arbman, M. *J. Electron Spectrosc. Relat. Phenom.* **1986**, *40*, 163.

Table 2a. Calculated Lowest Electron Binding Energies of Aqueous Cations, $E_{\text{aq}}^{\text{charges}}$, $E_{\text{aq}}^{\text{PCM}}$, and $E_{\text{aq}}^{\text{thermo}}$, Using Different Models (see text) Compared with Experimental Energies, $E_{\text{aq}}^{\text{PES}}$ (experimental (E_{g}) and calculated ($E_{\text{g}}^{\text{cal}}$) gas-phase ionization energies are also shown)

cation		$E_{\text{g}}(\text{M}^+)$ (eV)	$E_{\text{g}}^{\text{cal}}(\text{M}^+)$ (eV)	$E_{\text{aq}}^{\text{PES}}(\text{M}^+)$ (eV)	$E_{\text{aq}}^{\text{charges}}(\text{M}^+)^{\text{a}}$ (eV)	$E_{\text{aq}}^{\text{PCM}}(\text{M}^+)$ (eV)	$E_{\text{aq}}^{\text{Bom}}(\text{M}^+)^{\text{b}}$ (eV)
Li	1s	75.64 ^c	75.19 Δ CCSD(T) 75.10 Δ MP2	60.4 \pm 0.07		62.23 Δ CCSD(T) 62.13 Δ MP2	60.95
Na	2p	47.28 ^c 47.45 ^c	46.77 Δ CCSD(T) 46.82 Δ MP2	35.4 \pm 0.04		39.55 Δ MP2	35.70
K	3p	31.62 ^c 31.89 ^c	31.39 Δ CCSD(T) 31.54 Δ MP2	22.2 \pm 0.06		20.21 Δ CCSD(T) 20.37 Δ MP2	22.29
Rb	4p	27.29 ^c	27.58 Δ CCSD(T) 27.68 Δ MP2	not observed		18.93 Δ CCSD(T) 19.03 Δ MP2	18.66
Cs	5p	23.14 ^d	23.45 Δ CCSD(T) 23.45 Δ MP2	not observed		15.56 Δ CCSD(T) 15.56 Δ MP2	15.52

^a From average of three $p \rightarrow s$ components; 500 (1000) snapshots for Na^+ , Rb^+ (K^+ , Li^+). ^b $E_{\text{aq}}^{\text{thermo}}$ values assume that free energy of solvation of double cation is 3 times the single cation (see text). Solvation free energies for singly charged cations are from ref 80. ^c From ref 77. ^d From ref 78.

Table 2b. Calculated Lowest Binding Energies of Aqueous Anions, $E_{\text{aq}}^{\text{charges}}$, $E_{\text{aq}}^{\text{PCM}}$, and $E_{\text{aq}}^{\text{thermo}}$, Using Different Models (see text) Compared with Experimental Energies, $E_{\text{aq}}^{\text{PES}}$ (experimental (E_{g}) and calculated ($E_{\text{g}}^{\text{cal}}$) gas-phase ionization energies are also shown)

anion		$E_{\text{g}}(\text{A}^-)$ (eV)	$E_{\text{g}}^{\text{cal}}(\text{A}^-)$ (eV)	$E_{\text{aq}}^{\text{PES}}(\text{A}^-)$ (eV)	$E_{\text{aq}}^{\text{charges}}(\text{A}^-)^{\text{a}}$ (eV)	$E_{\text{aq}}^{\text{PCM}}(\text{A}^-)$ (eV)	$E_{\text{aq}}^{\text{Bom}}(\text{A}^-)^{\text{b}}$ (eV)
F	2p	3.40, ^c 3.45 ^d	3.31 Δ CCSD(T) 3.64 Δ MP2	8.7, ^e 9.8 ^f		7.8 Δ CCSD(T) 8.09 Δ MP2	8.3
Cl	3p	3.61, ^c 3.72 ^d	3.50 Δ CCSD(T) 3.63 Δ MP2	9.6 \pm 0.07		8.67 Δ MP2	7.3
Br	4p	3.36, ^c 3.82 ^d	3.39 Δ CCSD(T) 3.49 Δ MP2	8.8 \pm 0.06		8.19 Δ MP2	6.9
I	5p	3.06, ^c 4.00 ^d	3.09 Δ CCSD(T) 3.14 Δ MP2	7.7 \pm 0.20, 8.8 \pm 0.20		7.20 Δ MP2	6.1

^a From average of three $p \rightarrow s$ components. 500 (1000) snapshots for Cl^- , Br^- , (F^- , I^-). ^b $E_{\text{aq}}^{\text{thermo}}$ values assume free energy of solvation of the neutral is zero (see text). Solvation energies for anions are from ref 80. ^c From ref 79. ^d From sum of atomic transition line⁷² and gas-phase electron affinity.⁷⁹ ^e From ref 66. ^f Estimated from ref 65.

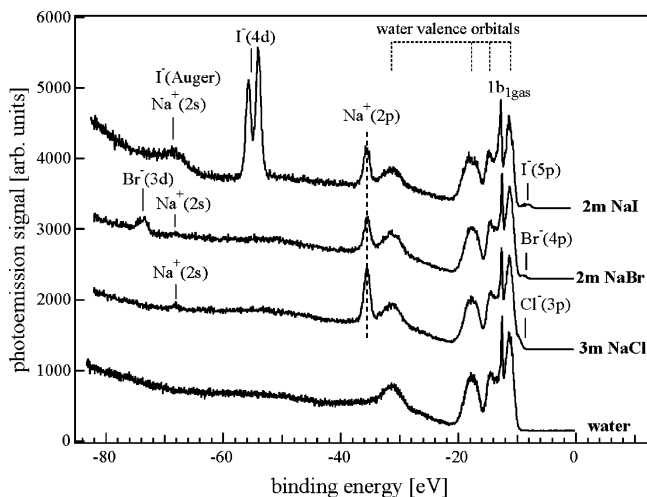


Figure 1. Photoemission spectra of pure liquid water, 3 m NaCl, 2 m NaBr, and 2 m NaI aqueous solutions, obtained from 100 eV photon energy. Electron binding energies are given with respect to the vacuum level, and intensities are normalized to the synchrotron photon flux. Emission from the water valence orbitals and from aqueous ions is labeled; the subscript gas denotes gas-phase water signal.

35.4 eV electron binding energy, $E_{\text{aq}}^{\text{PES}}$, for $\text{Na}^+(2s)$ and $\text{Na}^+(2p)$, respectively. There is some iodide Auger contribution overlapping with the $\text{Na}^+(2s)$ feature.⁶⁰ The Auger process is assigned to filling the $\text{I}^-(4d)$ hole by an $\text{I}^-(5p)$ electron and simultaneous emission of a $5p$ electron leading to a two-hole final state ($4d-5p5p$). The observed binding energies in Figure 1 are found to be independent of the counteranion for the concentrations studied. Furthermore, as reported previously for aqueous NaI solutions,⁶⁰ the energies of both anions and cations are constant for concentrations from 0.1 to 12.0 m NaI. The

exceptionally large $\text{I}^-(4d)$ signal intensity is due to a shape resonance peaking near 100 eV excitation energy.^{60,64}

Concentration variations for the chloride and bromide solutions were not performed below 0.5 m due to the low anion intensities. The energies of the aqueous anions in Figure 1 are 9.6 (8.7) eV ($\text{Cl}^-(3p)$), 8.8 (8.1) eV ($\text{Br}^-(4p)$), 73.2/74.3 eV ($\text{Br}^-(3d)$), 7.7/8.8 (7.3) eV ($\text{I}^-(5p)$), and 53.8/55.5 eV ($\text{I}^-(4d)$), where the pairs of numbers correspond to different spin-orbit states. Numbers in parentheses are the threshold energies obtained by linear extrapolation of the high-energy edge of the spectra in Figure 1; these values agree with previous reports on threshold measurements:³³ 8.77, 7.95, and 7.21 eV for $\text{Cl}^-(3p)$, $\text{Br}^-(4p)$, and $\text{I}^-(5p)$, respectively. Experimental electron binding energies ($E_{\text{aq}}^{\text{PES}}$) and peak widths ($\text{fwhm}_{\text{aq}}^{\text{PES}}$) of the aqueous cations and anions, determined by Gaussian peak fitting of the spectra, are summarized in Tables 1a and 1b.

Constant electron binding energies of a given solute anion are also observed for any of the anion/cation combinations. This is seen in Figures 2–4, presenting a series of photoemission spectra of aqueous alkali–chloride, alkali–bromide, and alkali–iodide aqueous solutions, again measured at 100 eV photon energy. Salt concentrations are as indicated, and peaks in the spectra are assigned by labels. The alkali–bromide series (Figure 3) is less complete, missing LiBr, and also lower concentrations were used. The lower CsI concentration in Figure 4 is used because the maximum solubility in water is less than 3 m. Fluoride salt solutions were previously investigated^{65,66} and have not been measured here. For completeness, Table 1b also

(64) Amusia, M. Y.; Cherepkov, N. A.; Chernysheva, L. V.; Manson, S. T. *Phys. Rev. A* **2000**, *61*, 020701.

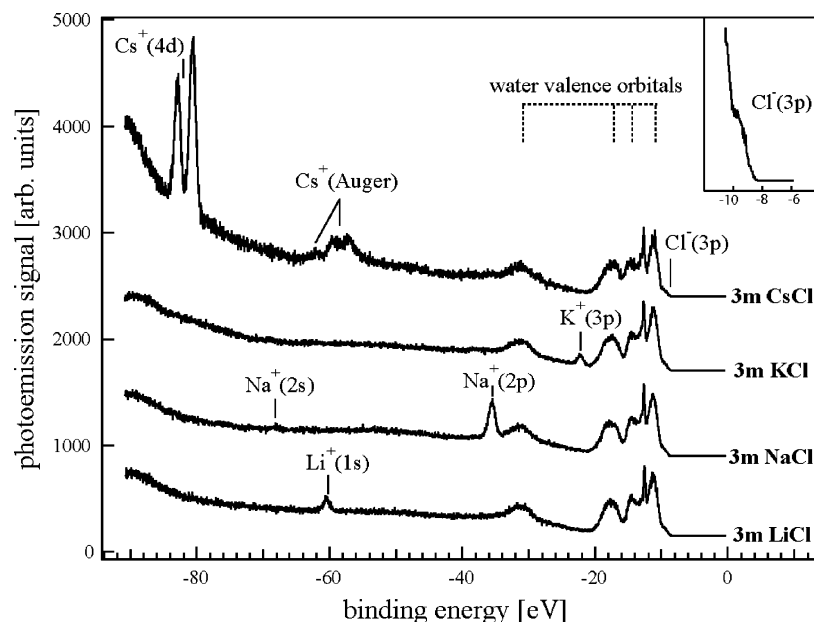


Figure 2. Photoemission spectra of aqueous alkali–chloride solutions (LiCl, NaCl, KCl, CsCl) obtained for 100 eV photon energy. The (molal) concentrations are given, and characteristic emission lines are labeled. The inset is an enlargement of the emission onset. Energies are with respect to vacuum.

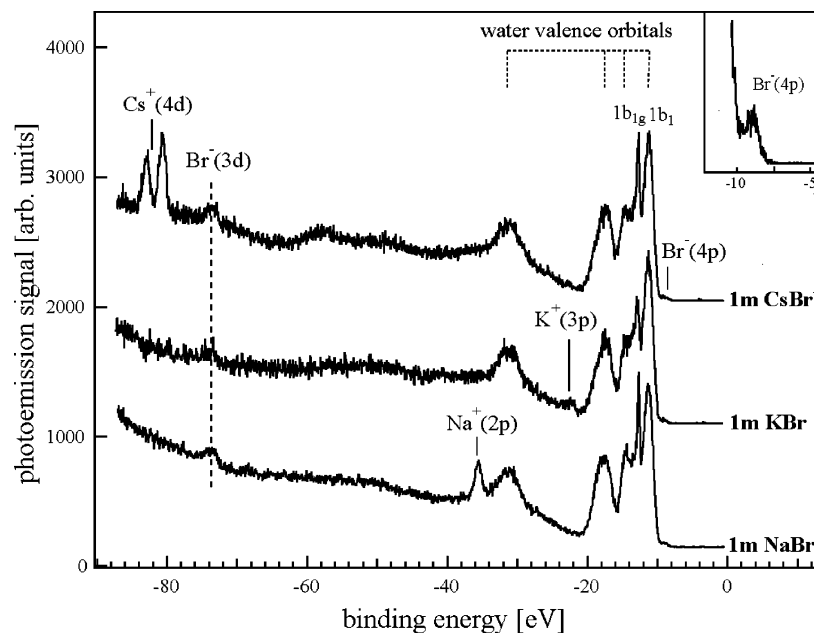


Figure 3. Photoemission spectra of aqueous alkali–bromide solutions (NaBr, KBr, CsBr) obtained for 100 eV photon energy. Molal concentrations are given, and characteristic emission lines are labeled. The inset is an enlargement of the emission onset. Energies are with respect to vacuum.

contains binding energies for fluoride estimated from refs 65 and 66. We note that the respective experimental values are rather inaccurate, differing by > 1 eV for the two studies, which results from the strong spectral overlap of the $F^-(2p)$ feature with the water $1b_1$ orbital emission. As to rubidium, only one salt solution, 3 m RbBr, was measured in the present experiment (not shown). No reliable experimental value of the $Rb^+(4p)$ energy could be inferred due to both the low photoionization cross section and the strong spectral overlap with the high energy side of the water $1b_2$ emission feature (liquid and gas phase).

For aqueous Li^+ , only the $Li^+(1s)$ line at 64.4 eV is observed. Two features are observed for aqueous K^+ , the $K^+(3p)$ emission at 22.2 eV and very weak $K^+(3s)$ emission at 38 eV. Cs^+ again only exhibits one distinct feature, an intense doublet at 80.6/82.9 eV, arising from $Cs^+(4d)$ emission. This peak is nearly as intense as that of the $I^-(4d)$ peak. In addition, cesium Auger emission, $Cs(4d-5p5p)$, gives rise to the feature near 58 eV,⁶⁰ which is best observed in Figure 2 and barely seen underneath the $I^-(4d)$ signal in Figure 4. No $Cs^+(5p)$ and $Cs^+(5s)$ signal is found in our spectra because of the expected spectral overlap with the water valence features and also due to low photoionization cross sections. In fact, the neutral gas-phase alkali atoms, $Cs(5p)$ and $Cs(5s)$, have the lowest photoionization cross sections, lower than that for $K(3s)$ at 100 eV.⁶⁷ Measured

(65) Faubel, M. Photoelectron Spectroscopy at Liquid Surfaces. In *Photoionization and Photodetachment*; Ng, C. Y., Ed.; World Scientific: Singapore, 2000; Vol. 10A, Part 1, p 634.

(66) Bohm, R.; Morgner, H.; Oberbrodthage, J.; Wulf, M. *Surf. Sci.* **1994**, *317*, 407.

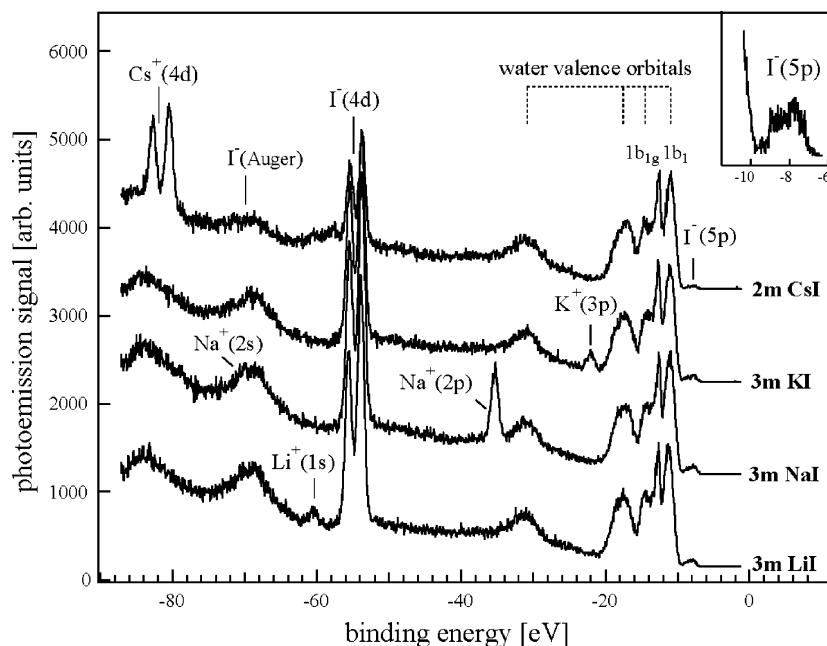


Figure 4. Photoemission spectra of aqueous alkali-iodide solutions (LiI, NaI, KI, CsI) obtained for 100 eV photon energy. Molal concentrations are given, and characteristic emission lines are labeled. The inset is an enlargement of the emission onset. Energies are with respect to vacuum.

ionization energies and peak widths from Figures 2–4 are also summarized in Tables 1a and 1b for cations and anions, respectively. Again, these numbers do not depend on the counterion used. Also notice that the binding energies presented are independent of the photon energy, at least for 60, 80, and 100 eV used here (the lower energies would, of course, be insufficient to ionize all levels listed in the tables).

B. Calculated Electron Binding Energies: Aqueous Cations. The computed gas-phase ionization energies of the complete series of alkali cations perfectly (within $\sim 1\%$) reproduce the experimental values (see first two columns in Table 2a). Convergence is reached already at the MP2 level, which gives IEs within 0.1 eV from the CCSD(T) values. The validity of the single reference approach was further verified by CASSCF calculations, yielding electron binding energies very close to the MP2 or CCSD(T) values. This gives us confidence that the electronic structure of the atomic ion is well described prior to probing solvent interactions.

The vertical ionization energies (VIEs) of aqueous alkali cations were evaluated at the MP2 level employing either explicit solvent (with geometries taken from MD simulations and water molecules represented as fractional charges) or a polarizable continuum solvent model (see columns 4 and 5 in Table 2a). We note that, as for the gas-phase result, going from MP2 to CCSD(T) with the continuum solvent has little effect on the VIE. We assume that correlation contributions are nearly converged and carry out the explicit solvent computation at the less expensive MP2 level to allow averaging over a large number of solvent configurations.

The ab initio VIEs can be compared to those estimated from the simple thermodynamic treatment outlined in section B.2 as well as to experiment (Table 2a). We see that the thermodynamic $E_{\text{aq}}^{\text{Born}}$ and PCM models perform very well, despite the fact that they, strictly speaking, provide adiabatic rather than vertical

ionization energies. However, the explicit solvent model systematically overestimates the VIEs by more than 10%. The likely cause of the differing performance of each solvent model will be discussed in the next section. Our best estimates for the lowest VIEs of Rb^+ and Cs^+ are thus 18.66 and 15.52 eV, respectively. In both cases, features due to these processes are likely to be buried under the liquid water valence peaks in the experimental spectrum.

Despite overshooting the magnitude of the vertical ionization energies, the explicit solvent model allows us to consider the effect of the range of thermally populated cation solvation structures, as well as the effect of p orbitals degeneracy lifting by the asymmetry of these solvent structures, on the width of the photoelectron band. Figure 5 (left) shows the simulated photoelectron band for ionizing Na^+ . The overall peak width (1.1 eV) is in good agreement with that of experiment. Most of the broadening of the band arises from inhomogeneous broadening, due to the variety of solvent configurations thermally sampled. The agreement with experiment provides evidence that the force field model for the equilibrium molecular dynamics simulation is a satisfactory representation of the solvent interactions with the sodium ion. The splitting of the Na^+ p orbitals due to the asymmetric distribution of the surrounding waters is rather small, ~ 0.03 eV. For lithium, ejection takes place from an s orbital, and thus the simulated peak is broadened (total width = 1.24 eV) only by different solvent configurations. For the remaining cations, the splitting due to degeneracy lifting increases, but the overall widths of the photoelectron bands are approximately constant; the overall widths and splittings are 1.07 and 0.05 eV (K^+), 1.07 and 0.08 eV (Rb^+), and 1.05 and 0.1 eV (Cs^+).

In addition to computing the lowest vertical ionization energies, where the metal cation p orbital electron is ejected, we can come up with estimates for the ionization energy of the deeper lying s orbital. We note that this direct quantity has not, to the best of our knowledge, been measured for gas-phase alkali

(67) Yeh, J.-J. *Atomic Calculations of Photoionization Cross Sections and Asymmetry Parameters*; Gordon and Breach: Langhorne, PA, 1993.

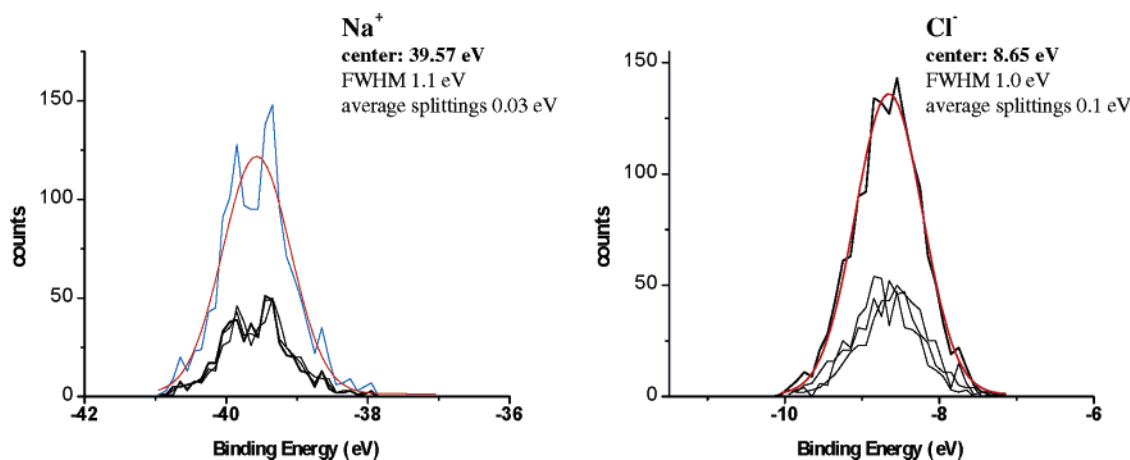


Figure 5. Histogram representing the photoelectron spectrum for aqueous (left) Na^+ and (right) Cl^- built from 500 molecular dynamics snapshots. The band shape is decomposed into underlying ejection from each of the three degeneracy-lifted p orbitals (average splitting shown). The combined line shape is fit to a Gaussian for which the full width at half-maximum (fwhm) and peak center are given.

Table 3. Gas-Phase Atomic $ns \rightarrow np$ Excitation Energies for Alkali Dications and Halide Anions^a

	B3LYP	experiment
Na^{2+}	31.64	32.8 ^b
K^{2+}	17.11	16.19 ^b
Rb^{2+}	15.04	
Cs^{2+}	13.85	
F	20.64	20.89 ^c
Cl	12.33	
Br	11.91	10.51 ^b
I	10.50	10.17 ^b

^a These experimental and computed values are useful to assign deeper level electron ejection energies for the aqueous ions. Anion basis sets are cc-pVTZ (or equivalent), and cation basis sets are Na^{2+} cc-p5Z and K^{2+} 6-311g(2d,f), Cs^{2+} WTBS (well-tempered basis set).⁵⁴ ^b From ref 77. ^c From atomic transition line.⁷²

cations. These estimates are solely to provide a guide for where such an ejection process would be expected to appear in the liquid-phase EUV photoelectron spectrum. The ionization energies are estimated as the sum of the solution phase ionization energy from the np orbital ($E_{\text{aq}}^{\text{PES}}$) plus the $ns \rightarrow np$ excitation energies for the dications. The latter quantities, computed using a TD-DFT approach for the gas-phase dication compared with relevant gas-phase experimental data are shown in Table 3. We note that the TD-DFT values are in most cases in good agreement with experimental data where available, indicating that the $ns \rightarrow np$ excitation can be described by such a relatively simple approach since it is essentially of a one-electron nature. It is reasonable to use the gas-phase excitation energy for M^{2+} in this overall procedure as the solvent configuration remains constant for the overall vertical process from M^+ . By summing values from Table 3 and Table 2a, we estimate s orbital vertical ionization features at 68.2 (Na^+) and 38.4 eV (K^+), which provides assignment for the peaks observed in Figures 1 and 2 at 68.0 and ~ 38 eV, respectively, and predicts features in the spectra of Rb^+ at 34.0 eV and of Cs^+ at 29.4 eV (using thermodynamic cycle and B3LYP numbers in each case). These features are likely to be difficult to observe due to the strong broad water valence peak centered at 32 eV (see Figures 2–4 and ref 19).

C. Calculated Electron Binding Energies: Aqueous Anions. As for the alkali cations, the gas-phase electron affinities (EA) of the halide anions are accurately reproduced at the CCSD(T) level. At the MP2 level, the EA is overestimated by

0.1–0.3 eV. When we consider the effect of solvent on the VDE, however, we see that the two continuum treatments that performed well for cations are rather unsatisfactory for the anions. Neither the VDE estimate based on the free energy of halide solvation nor the ab initio polarizable continuum model account for the solvation effect on detachment energetics; both underestimate experiment by around 2 eV (see third and last two columns in Table 2b). This might be expected as both methods provide adiabatic energies, while photoemission measurements correspond to vertical detachment energies. The explicit solvent model, which employs snapshots from MD simulations and point charge representations of water molecules, and which provides vertical detachment energies, performs much better (see columns 4 and 5 in Table 2b). Although this approach still underestimates the VDE, e.g., for iodide, we are within 0.5 eV. It is worthwhile noting that this model predicts a lower bound estimated VDE for fluoride of 11.2 eV (well above two experimental results reported elsewhere at very high fluoride concentrations^{65,66}). A photoelectron peak due to detachment of F^- should be buried under the water $1b_1$ valence feature, which appears at the same energy.

As for the cations, the explicit solvent model also allows simulation of the experimental photoelectron band as well as consideration of the origin of the observed peak width. Figure 5 (right) shows the simulated photoelectron band for detaching Cl^- . The simulated peak width (1.04 eV) is considerably larger than the experimental width (0.6 eV). Most of the broadening of the band is again due to inhomogeneous broadening as a result of thermally populated solvent configurations, although the splitting of the Cl^- p orbitals due to the asymmetric distribution of the surrounding waters is larger than that for Na^+ (~ 0.11 eV). For the remaining anions, the splitting due to degeneracy lifting increases slightly, but the overall widths of the photoelectron bands decrease slightly as one moves down the halogen group; the overall widths and splittings are 1.08 and 0.12 eV (F^-), 0.96 and 0.12 eV (Br^-), and 0.94 and 0.13 eV (I^-). Although the simulated widths are larger than experimentally observed (Tables 1a and 1b), they are consistent with the experimental trend that halides exhibit narrower photoelectron bands than do the alkali cations.

Once again, we can derive estimates for the detachment energies of deeper lying s orbitals of the various halides studied

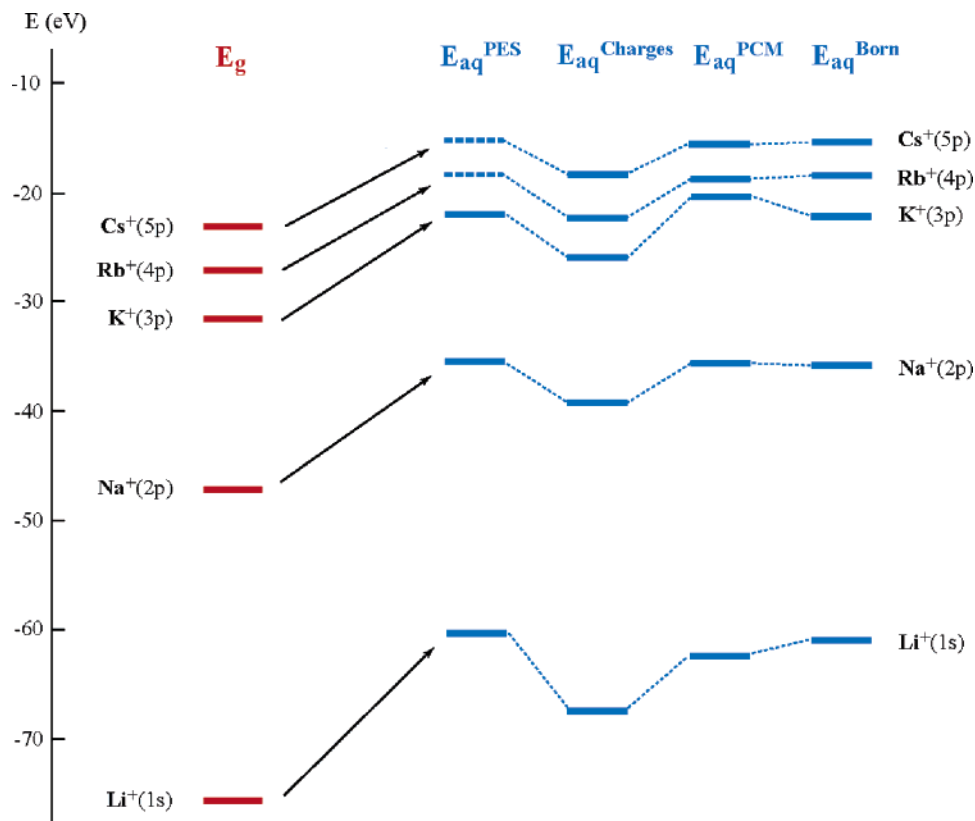


Figure 6. Diagram of lowest electron binding energies of gas-phase cations (E_g) and of the respective aqueous cations (E_{aq}). Energy values are from Tables 1a and 2a. For Cs and Rb (dotted lines), no accurate experimental E_{aq} values could be inferred in the present study.

in order to predict where such ejection processes should appear in the liquid-phase EUV photoelectron spectrum. Again, this quantity has not been measured for halide anions in the gas phase, where the photon energy rarely exceeds 6.4 eV. The detachment energies are estimated as the sum of the solution-phase detachment energy from the np orbital (E_{aq}^{PES}) plus the ns \rightarrow np excitation energies for the halogen neutral (Table 3). By summing values from Table 3 and Table 2b, we predict s orbital vertical detachment features at 21.9 (Cl⁻), 19.3 (Br⁻), and 17.9 eV (I⁻). The chloride feature should not be obscured by the \sim 18 eV water valence band. None of these detachment processes are, in fact, resolved in the experimental spectra (see Figures 1–4), suggesting that the photodetachment cross section for s orbital detachment is lower than that for the equivalent process in alkali cations.

IV. Discussion

Figures 6 and 7 graphically depict the highest occupied orbital electron binding energies of gas-phase ions (E_g) and of the respective aqueous ions (E_{aq}). Also shown are the various calculated energies, $E_{aq}^{charges}$, E_{aq}^{PCM} , E_{aq}^{Born} . One notices that E_{aq}^{PES} for cations (M^+ , Figure 6) are smaller than the respective E_g , while the opposite is true for aqueous anions (A^- , Figure 7): $E_{aq}^{PES}(M^+) < E_g(M^+)$ and $E_{aq}^{PES}(A^-) > E_g(A^-)$, the energy difference being considerably larger for cations though. This behavior can be directly related to the respective expressions for $\Delta G_f^{cav} - \Delta G_i^{cav}$ deduced in section B.2. It is particularly interesting that the electron binding energies seem to be insensitive to the nature of the counterion (even at the relatively high concentrations these experiments were recorded at) and to the concentration of the solute. Similar insensitivity to the

salt environment has been observed in the electron detachment dynamics from anions where the detached electron remains trapped in the liquid phase. Contrary to expectations based on Debye–Hückel picture, significant effects are only observed when the salt concentration approaches 5 m.^{25,68}

As displayed in Table 2a, both adiabatic models give good results for energies of aqueous cations; the best match with the experiment (within 0.5 eV) is in fact always obtained for the simple thermodynamic cycle model (see section B.2), which considers the experimental solvation free energies, ΔG° , only. The situation is reversed for aqueous anions; here, the ab initio treatment with explicit charges for the structured solvent shells, $E_{aq}^{charges}$, agrees best with the experimental energy, but it still underestimates the experiment by 0.5–1.0 eV. Results are better for the larger anions. For anions, the E_{aq}^{PCM} and E_{aq}^{thermo} values systematically underestimate the experimental binding energies by 1.5–2.5 eV.

Why do the simple Born and PCM models work so well for cations but poorly for anions? Both models provide adiabatic rather than vertical ionization energies. In contrast, the explicit solvent model is vertical with respect to nuclear polarization (the orientation of the waters), so why does it fail for the cation binding energies? Our results indicate that the change from (mono)cation to equilibrium dication is accompanied by only a minor change of water geometry, at least at short range, the solvent is already favorably preoriented around the cation, and any additional longer range ordering of the water dipoles in response to the charge change does not significantly contribute to the energy. On the other hand, the explicit charges model

(68) Lian, R.; Crowell, R. A.; Shkrob, I. A.; Bartels, D. M.; Oulianov, D. A.; Gosztola, D. *Chem. Phys. Lett.* **2004**, *389*, 379.

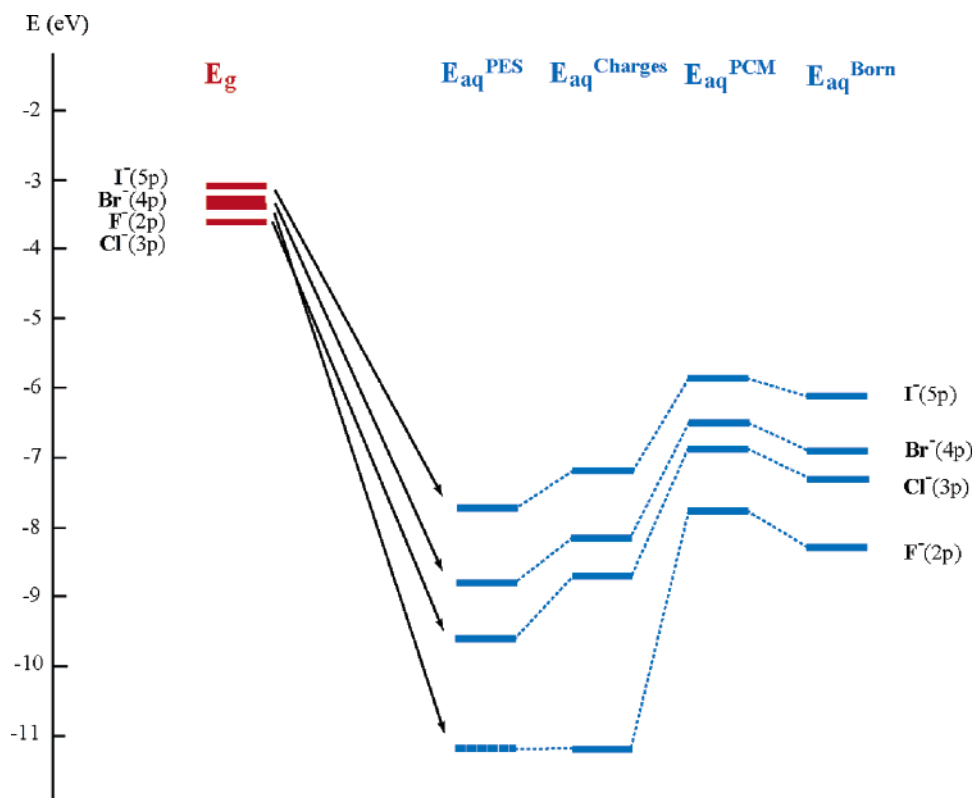


Figure 7. Diagram of detachment energies of gas-phase anions (E_g) and of the respective aqueous anions (E_{aq}); compare Tables 1b and 2b. The dotted line for $F^-(2p)$ reproduces the respective $E_{aq}^{charges}$ value; E_{aq}^{PES} for F_{aq}^- was not measured here.

overestimates the electron binding energy, and although relaxation of the water dipoles is properly prohibited, mirroring the instantaneous ionization event, the approach is missing the change in electronic polarization of the water. Water molecules represented as point charges cannot be polarized, and electron cloud polarization interactions are always stabilizing. The polarization effects are present already for monovalent ions; however, they become particularly strong in the case of multivalent ions. Indeed, the strong electric field of the dication polarizes the surrounding water molecules more than that of the monocation. As a result, the explicit charge model, which cannot reproduce the differential electronic polarization, tends to overestimate the electron VDE from the alkali cation. In our previous study on hydrated iodide,²⁹ we accounted for the main part of this polarization effect, which is relatively small for singly charged ions, such as I^- , and even smaller for the corresponding neutral species by including the first solvation shell water molecules with their full electronic structure (i.e., not merely as point charges) into the *ab initio* calculations. Unfortunately, this approach cannot be directly applied for the alkali cations. If one includes the electronic structure of the first solvation shell water molecules into the *ab initio* calculation, then the lowest IP would correspond to water ionization rather than that of Na^+ . The desired ionization of the sodium cation would then correspond to a highly excited state of the whole system which would be very difficult to evaluate accurately.

On the contrary, for halide anions, electron detachment results in a significant reorientation of the solvation shell; water molecules prefer to point with hydrogen atoms toward the anion but with oxygen atoms toward neutral halogen atoms. In addition, there is no strong change in the electronic polarization of the surrounding water molecules by the formation of the

neutral halogen atom. Therefore, for the anions, it is more important to have a vertical treatment of the nuclear polarization, which also rationalizes the poor performance of adiabatic continuum models.

Despite achieving this vertical description within the explicit solvent model, the calculations in the presence of a bulk charge field still systematically underestimate the VDE for the halide anions exciting from the valence p orbital (see Table 2b). Even for iodide, $E_{aq}^{charges}$ is 0.5 eV too low. We consider several sources for this error. Including the first solvent shell (typically 6–8 waters) quantum mechanically, on average, increased the binding energy by ~ 0.2 eV.²⁹ This test not only assesses the quality of the approximation of employing simple charges at the atomic positions for all waters but also quantifies the assertion in the last paragraph, giving us an estimate for the effect of neglecting the electronic polarization in the first shell in the computed VDE. We have also tested the convergence of the VDE with the number of solvent shells explicitly included in the charge field (i.e., examining how long range is the nuclear solvent polarization around the anion). Six shells (450 waters) are required to reach within 0.25 eV of the final total polarization, so the nuclear polarization is almost completely saturated in the current calculations for iodide, but a larger number of waters may be required for the more strongly solvated ions. Finally, we noticed in our earlier study a small difference in the vertical binding energy from iodide at the interface; as the anion is stabilized at the interface, the vertical detachment energy is greater by ~ 0.1 eV, compared to that of an ion in the bulk.²⁹ Overall, the combined effect of these four factors would be expected to bring the calculated VDE of aqueous iodide into reasonably close agreement with the experiment.

It is perhaps of interest to comment further on the sensitivity of the valence electron binding energies of anions to location in the surface or bulk as it appears that more polarizable anions may exhibit a propensity for existing at the surface layer.^{12,13} The photoelectron spectroscopy apparatus, as currently configured, in fact samples both bulk and interfacial iodide anions, so the peak in the photoelectron spectrum would be likely an average of the two. However, negligible differences in electron energy for surface versus bulk solvated iodide have been found in a comparative experimental study of aqueous NaI and surface-active tetrabutylammonium iodide (TBAI) aqueous solution.⁶⁹ For the latter, a single segregation surface layer is formed, with both anions and cations residing in the solution surface only.^{69,70} Hence, as opposed to simple salt solutions, the iodide photoemission signal in TBAI solution is sampled primarily from the very interface, despite the fact that no significant (beyond the resolution of the experiment) differences in iodide peak width and position were observed. Studies of the electron binding energy dependence on the photon energy, by which the probing depth can be varied, have not yet been attempted systematically for the aqueous solutions. In any case, the electron inelastic mean free path (IMFP) can be assumed to be not larger than 3–10 Å, at kinetic energies between 30 and 100 eV.⁷¹ Applied to water, this would correspond to about 1–3 layers. The actual IMFP is, however, not only energy dependent but also direction dependent, and in addition, it is governed by the particular electronic properties of the condensed phase material (surface). Notice though that reliable IMFPs for liquids and liquid water, in particular, are not available for the 30–100 eV energy range. For a typical solid, studied at normal emission angle (with respect to the surface), and assuming similar photoionization cross sections for surface and bulk species, the measured signal would roughly contain 20–30% surface contribution. We suggest that this is similarly true for liquid water and aqueous solutions, which brings up the question whether the peak energies measured here are bulk-representative. The answer tends to be yes for two reasons. First, as outlined above for iodide, the bulk and surface solvated anions are likely to have very similar binding energies; this also seems to be confirmed by the observed symmetric peak shapes and by previous calculations, which show that the VDEs for iodide in the aqueous bulk and at the surface differ by less than 0.1 eV.²⁹ Second, if hypothetically the surface effect would be responsible for the discrepancy between experimental and calculated values of binding energies for the anions (Table 2b), the agreement should be worse for iodide which, due to the largest polarizability, has the largest surface propensity. This is, however, not supported by our data.

The experimental photoelectron spectra also report on removal of electrons from deeper lying orbitals of the aqueous anions. In most cases, there is no direct corresponding data for the energies of these orbitals for the vacuum ions. We have made estimates for the binding energies for s orbital ejection for all cations and anions. In the cases where features are observed in the photoelectron spectra, the energy differences with the lowest energy ionization peak are in good agreement with gas-phase s

→ p excitation energies of the corresponding dications. For the remaining cations and all anions, either the predicted binding energies are close to a strong water feature in the photoelectron spectrum or the photoionization cross section must be low. In contrast, ionizing transitions from the d orbital appear for I⁻, Br⁻, and Cs⁺, and are particularly strong for Cs⁺ and I⁻. For comparison, the ratio of the photoionization cross sections of the neutral atoms Br(3d):I(4d):Cs(4d) is 1.9:5.8:9.3.⁶⁰ Equivalent theoretical estimates for these ejection energies are not computed as d → p excitations for the final state system lie in the continua of the respective species.

The experimental peak widths (see Table 1) tend to be noticeably larger for cations. Although the simulations employing the discrete charge model for the solvent reproduce this trend, the simulations slightly underestimate the width of the cation valence photoelectron bands while they consistently overestimate the bandwidth for the halides, particularly chloride. As the simulations do not fully include the homogeneous broadening due to solvent motion in the upper state, and neglect spin–orbit splitting in the final state, one would expect the theoretical peak shape to be too narrow in general. However, spin–orbit splitting is likely only significant for the observed case of bromine, where the peak splitting is unresolved but will add significant width (the gas-phase spin–orbit splitting is 0.457 eV).⁷² One would expect the major difference between anions and cations to be due to the sensitivity of the orbital energy to the solvent configuration. The highest occupied orbital for a cation is more tightly held to the nucleus, so one would expect it to be less solvent sensitive, but the overall orbital binding energy is also larger. Thus, in relative terms, the width ($\Delta E/E_{\text{aq}}^{\text{PES}}$) for cations is smaller than that for anions. Considering ejection from more tightly bound orbitals, the relative peak widths are smaller for the deeper lying d orbitals. For both anions and cations, the relative peak widths increase with increasing atomic number for ejection from a p orbital.

Finally, it is interesting to compare the vertical energies reported here to the energy diagram for liquid water when its electronic structure is treated within the formalism of solid-state physics.^{32,73} The magnitude of the band gap for liquid water has long been controversial,^{24,73} but the value for the vertical ionization energy from liquid water from the liquid photoelectron spectrum^{19,44} has helped to clarify the different energetic contributions to the adiabatic band gap.³² One can regard the anions and cations in solution as defects in a liquid insulator. The anions provide for mid-gap states, whereas the highest occupied orbital of each cation lies deeper than the valence band of water. The position of the aqueous halide anions on the band diagram for water has been discussed in detail in refs 32 and 74. This current work provides accurate vertical detachment energies in that endeavor. Further, comparison of the vertical energy to detach a valence electron to vacuum with the energy to promote the same electron to the polarization bound CTTS state is highly valuable as the two are expected to be correlated.⁷⁵ We expect that knowledge of the VDE for anions, where CTTS assignments (e.g., F⁻, NO₃⁻) have not been hitherto made, will be particularly useful. In the specific case of F⁻, it is currently

(69) Winter, B.; Weber, R.; Schmidt, P. M.; Hertel, I. V.; Faubel, M.; Vrbka, L.; Jungwirth, P. *J. Phys. Chem. B* **2004**, *108*, 14558.

(70) Vrbka, L.; Mucha, M.; Minofar, B.; Jungwirth, P.; Brown, E. C. *Curr. Opin. Colloid Interface Sci.* **2004**, *9*, 67.

(71) Pianetta, P. (<http://xdb.lbl.gov/section3>), March 2005.

(72) Moore, C. E. *Atomic Energy Levels*, 1971; Vol. INSRDS-NBS 35.

(73) Bernas, A.; Grand, D. *J. Phys. Chem.* **1994**, *98*, 3440.

(74) Coe, J.; Earhart, A. D.; Cohen, M. H.; Hoffmann, G.; Sarkas, H. W.; Bowen, K. H. *J. Chem. Phys.* **1997**, *107*, 6023.

(75) Takahashi, N.; Sakai, K.; Tanida, H.; Watanabe, I. *Chem. Phys. Lett.* **1995**, *246*.

unclear whether the VDEs obtained in previous measurements and reported in Table 3 are high enough when looking at the trends in the computed VDEs in going from chloride to fluoride. In fact, the strong spectral overlap of the $F^-(2p)$ and the liquid water $1b_1$ features and the lower count rates plus significant secondary electron background in the previous study⁶⁵ complicate the accurate assignment of the former binding energy.

In studies of aqueous anion photodetachment where the electron is ejected into the liquid, the failure to classify and compare the different experimental studies in terms of energetics has hampered the clear rationalization of mechanism. For example, for $I^-(aq)$, there is a 2.2 eV gap between the vertical CTTS transition and the vertical vacuum detachment energy. Careful inspection of Figure 4 shows the equilibrium anion is only optically coupled to the detachment continuum from above 6.5 eV. This means that for energies between 5.5 and 6.5 eV, detachment must take place indirectly via solvent rearrangement or by a nonadiabatic transition into the conduction band.³⁰ Even above 6.5 eV, one would expect an excitation energy varying pathway for production of e^-_{aq} . The experimental ejection dynamics on increasing the excitation energy across this range and the nature of CTTS resonances within the conduction band continuum have been recently explored.^{31,76}

Summary

We have presented a comprehensive study of theoretical and experimental vertical electron binding energies of aqueous alkali cations and halide anions. Experimentally, electron binding energies were directly measured using EUV photoelectron

spectroscopy of the respective salt aqueous solutions. No noticeable change of peak width or peak position of a given aqueous ion was observed in the photoemission spectra as a function of counterions and salt concentration; systematic photon energy variation has not yet been studied.

We have used different theoretical methods, accounting explicitly for the water solvent (via a fractional charge representation), through use of ab initio self-consistent reaction field (continuum) models and thermodynamic cycles using experimental hydration enthalpies. For cations, the thermodynamic cycles lead to an estimate within 0.1 eV or better of the experimental energies, but models based on ab initio methods, particularly those that attempt to compute the vertical binding energies, do more poorly. Treatment of both the electronic polarization and nuclear polarization difference between the initial and final states is clearly necessary to achieve a satisfactory description. Adiabatic thermodynamic cycles, however, fail even qualitatively to provide accurate estimates for the anion binding energies. For anions, it is more important for the nuclear polarization in the ground state to be correctly described, and not to relax this polarization in the final state. Reasonable estimates for the VDEs were obtained using an explicit charges method, with VDEs underestimated by as little as 0.5 eV. In addition to lowest electron binding energies, for some of the aqueous ions, electrons from deeper levels (including 4d) were detected, extending up to about 80 eV binding energy. We have made estimates for other deeper level ejections that were not observed in the experimental spectra due to overlap with strong water features and/or low ionization cross sections.

Acknowledgment. S.E.B. is supported by the David and Lucile Packard Foundation and the National Science Foundation (CHE-0311814). Computation for the work described in this paper was supported by the University of Southern California Center for High Performance Computing and Communications. Support from the Czech Ministry of Education via Grants LC512 and ME644, and from the US-NSF (CHE 0431512) is gratefully acknowledged. Part of the work in Prague was supported via the Research Project Z40550596.

JA042908L

- (76) Doucet, D.; Krylov, A. I.; Bradforth, S. E. In preparation.
(77) (a) Martin, W. C.; Fuhr, J. R.; Kelleher, D. E.; Musgrove, A.; Podobedova, L.; Reader, J.; Saloman, E. B.; Sansonetti, C. J.; Wiese, W. L.; Mohr, P. J.; Olsen, K. *NIST Atomic Spectra Database*, version 2.0; online: <http://physics.nist.gov/asd>; National Institute of Standards and Technology, Gaithersburg, MD, October 15, 2005. (b) Sansonetti, J. E.; Martin, W. C.; Young, S. L. *Handbook of Basic Atomic Spectroscopic Data*, version 1.1; online: <http://physics.nist.gov/Handbook>; Gaithersburg, MD, October 13, 2004.
(78) Benson, J. M.; Novak, I.; Potts, A. W. *J. Phys. B* **1987**, *20*, 6257.
(79) Lide, D. R. *Handbook of Chemistry and Physics*; CRC Press: Boca Raton, FL, 1997.
(80) Laidler, K. J.; Meiser, J. H.; Sanctuary, B. C. *Physical Chemistry*, 4th ed.; Boston, MA, 2003.